Electronic Supplementary Material (ESI) for Nanoscale.

Electronic Supplementary Information

Gas-assisted blade-coating of organic semiconductors: Molecular assembly, device fabrication and complex thin-film structuring

Hadhemi Mejri, Anika Haidisch, Peter Krebsbach, Mervin Seiberlich, Gerardo Hernandez-Sosa and Aleksandr Perevedentsev**

* gerardo.sosa@kit.edu and aperevedentsev@icmab.es

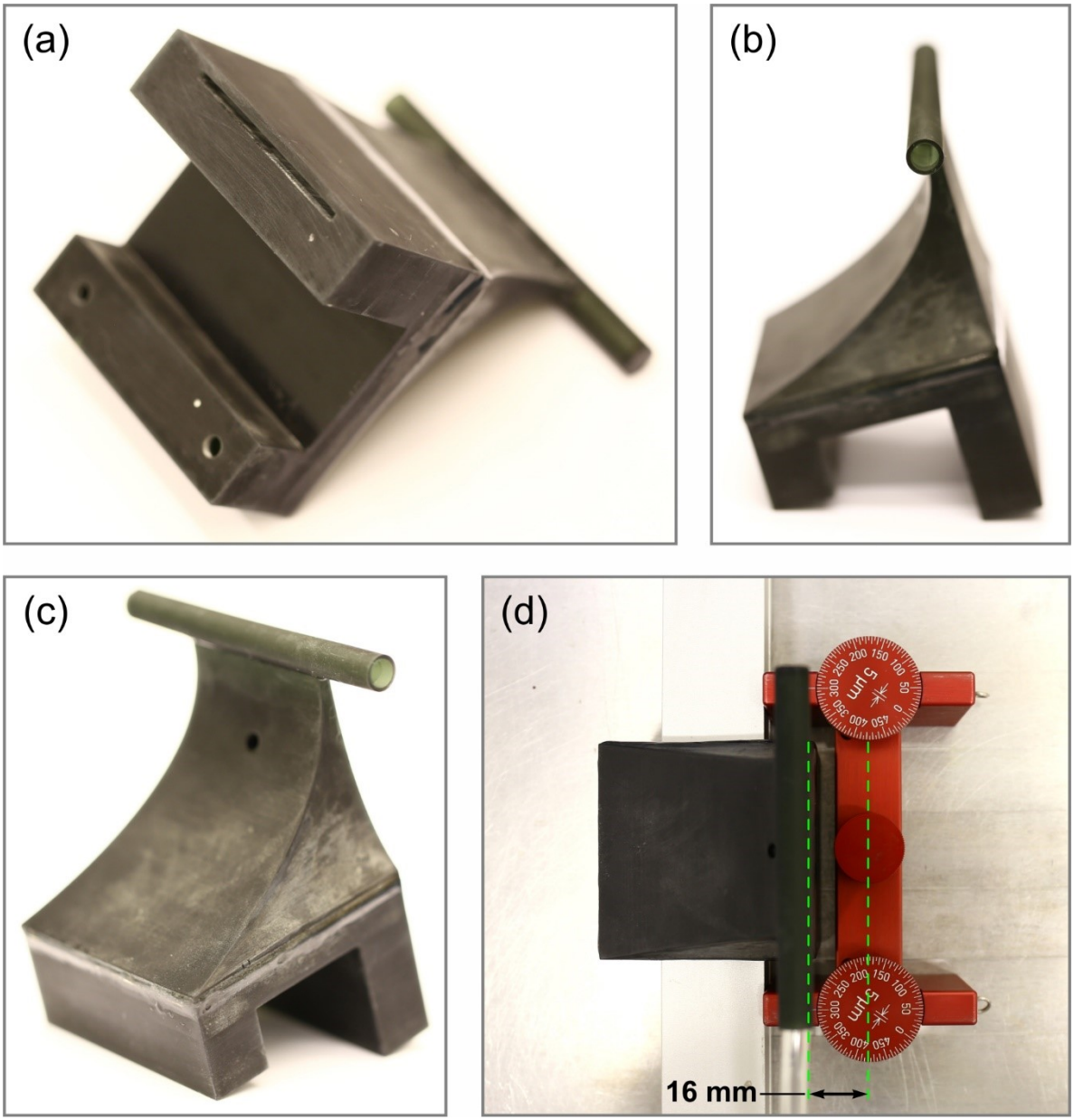

Figure S1. Images of the 3D-printed attachment used for gas-assisted blade-coating. As shown in (**d**), the distance between the slot-die directing the gas flow and the centre of the solution meniscus under the applicator is approximately 16 mm for the design used herein.

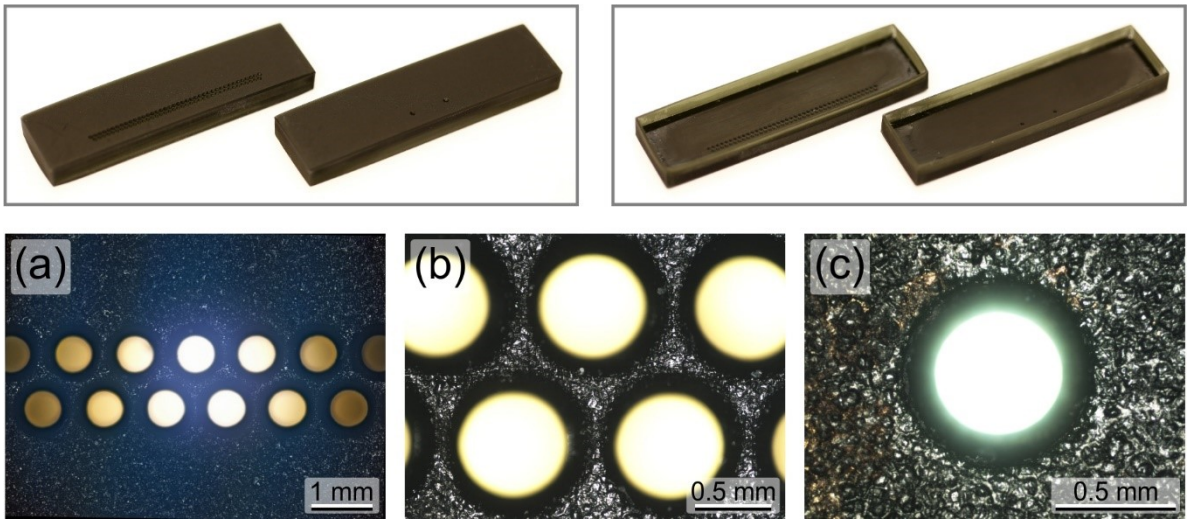

Figure S2. Exemplary nozzle adaptors for gas-assisted blade-coating: photographs and micrographs showing an expanded view of (**a,b**) an array of nozzles (0.75 mm diameter; left-hand photographs in the upper panel) and (**c**) an individual nozzle of a two-nozzle adaptor (0.75 mm diameter; right-hand photographs in the upper panel).

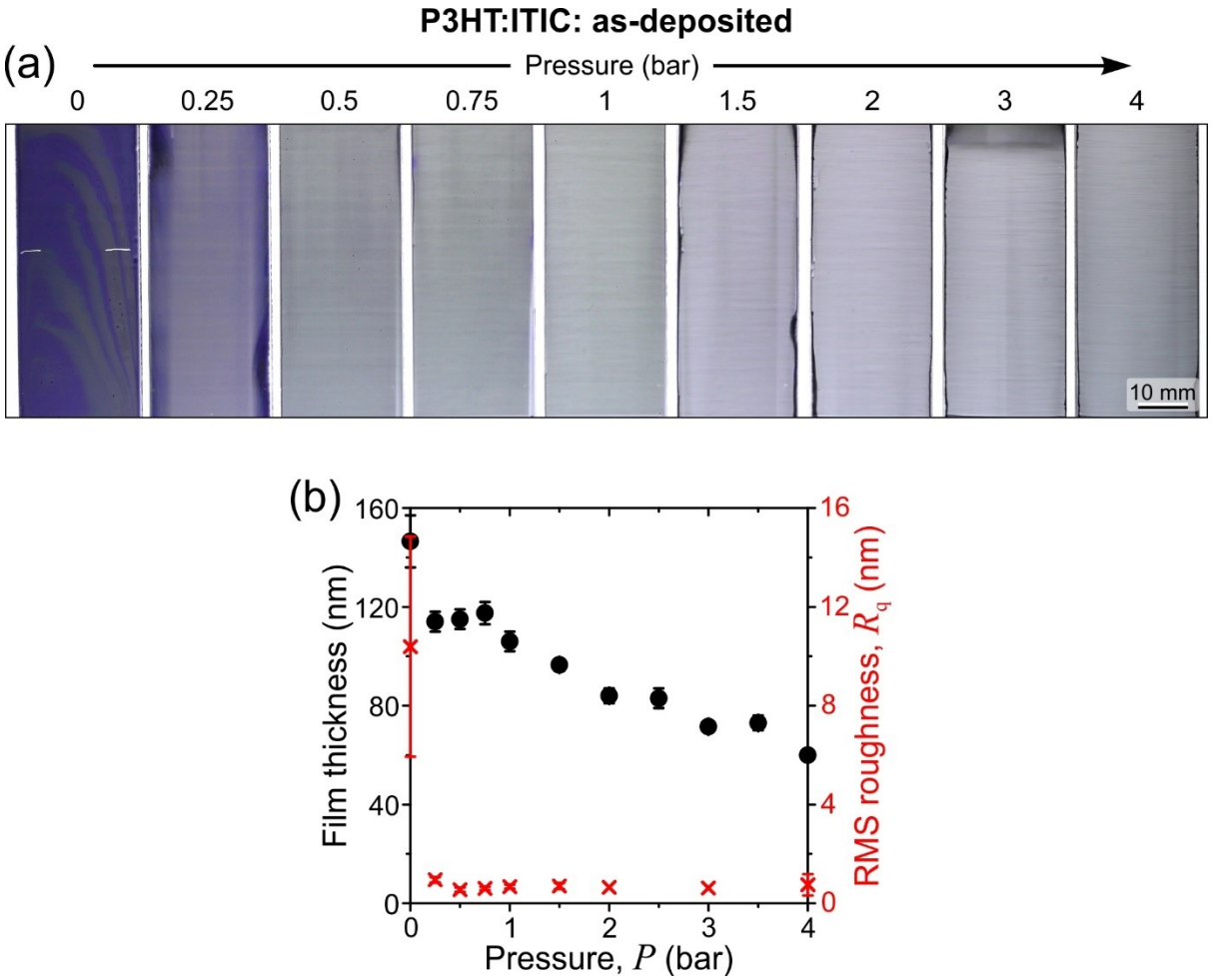

Figure S3. P3HT:ITIC films blade-coated at increasing gas pressures. (**a**) Transmitted-light images for as-deposited (non-annealed) films. (**b**) Thickness (*left ordinate*) and RMS roughness, R_q, (*right ordinate*) of the films as a function of pressure.

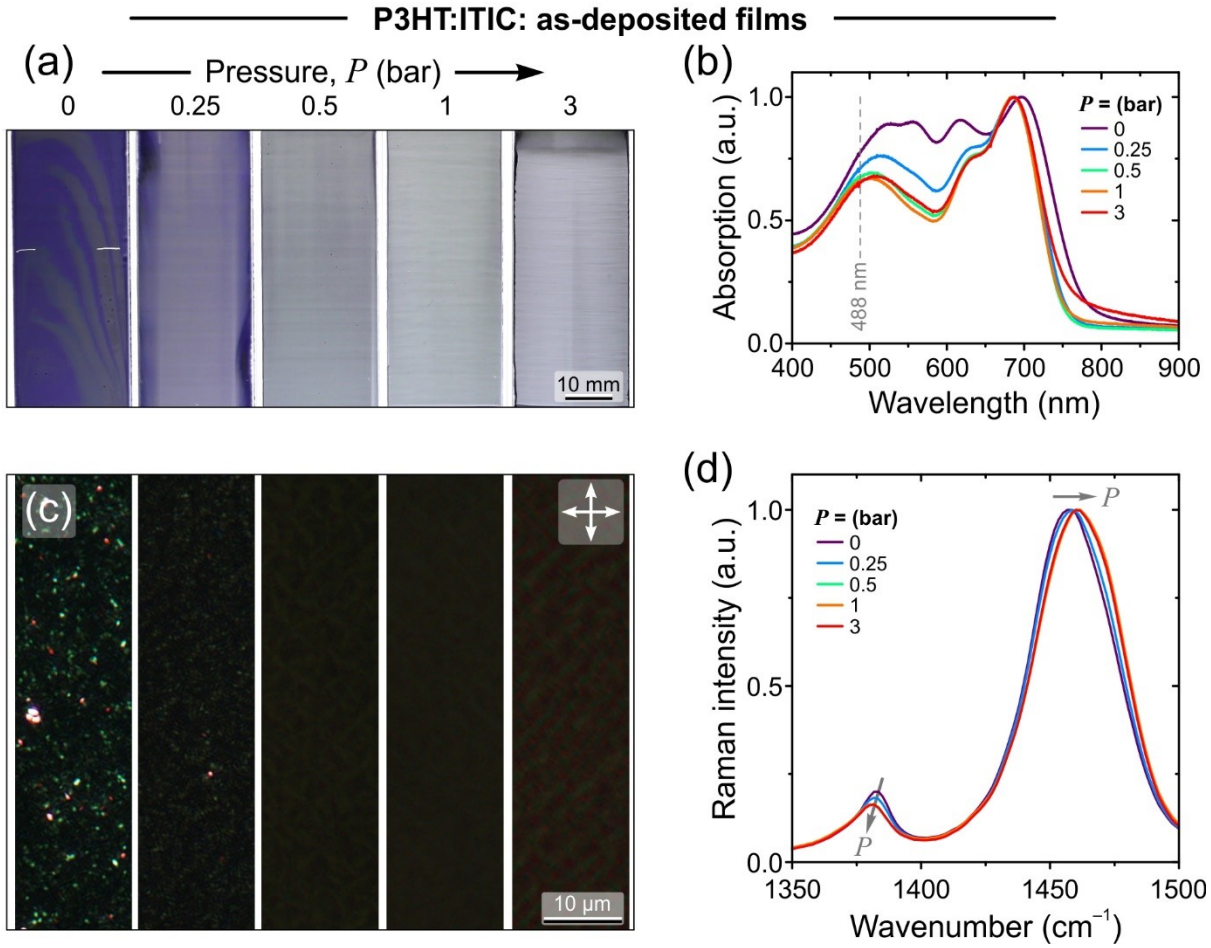

Figure S4. Suppression of crystallinity in P3HT:ITIC films blade-coated at increasing gas pressures. Data is shown for as-deposited films coated at the indicated gas pressures. (**a**) Transmitted-light images for selected films and the corresponding (**b**) peak-normalised absorption spectra, (**c**) cross-polarised micrographs and (**d**) expanded view of the Raman spectra centred on the C=C in-plane symmetric stretching mode of P3HT. In all cases, the data support the observation of P3HT:ITIC blend vitrification saturating for gas pressures ≥0.5 bar, namely: (a,b) the changes in light absorption characteristics, (c) the progressive disappearance of scattering centres in the cross-polarised micrographs and (d) the shift of the symmetric C=C stretch mode of P3HT to higher energies.

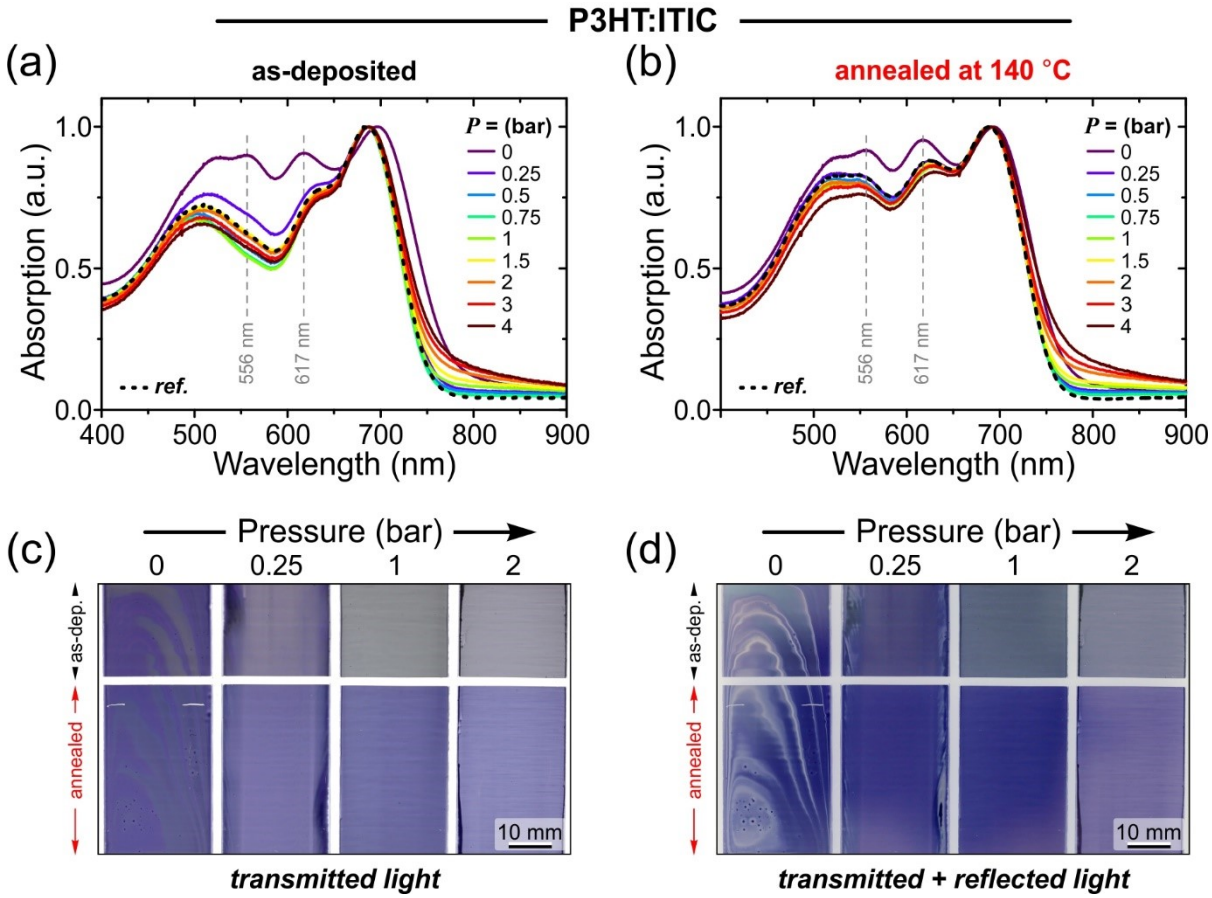

Figure S5. P3HT:ITIC films blade-coated at increasing gas pressures. Absorption spectra recorded for (**a**) as-deposited and (**b**) annealed P3HT:ITIC films. Also shown are the images of selected as-deposited (*upper panels*) and annealed (*lower panels*) films taken under (**c**) transmitted and (**d**) transmitted + reflected light.

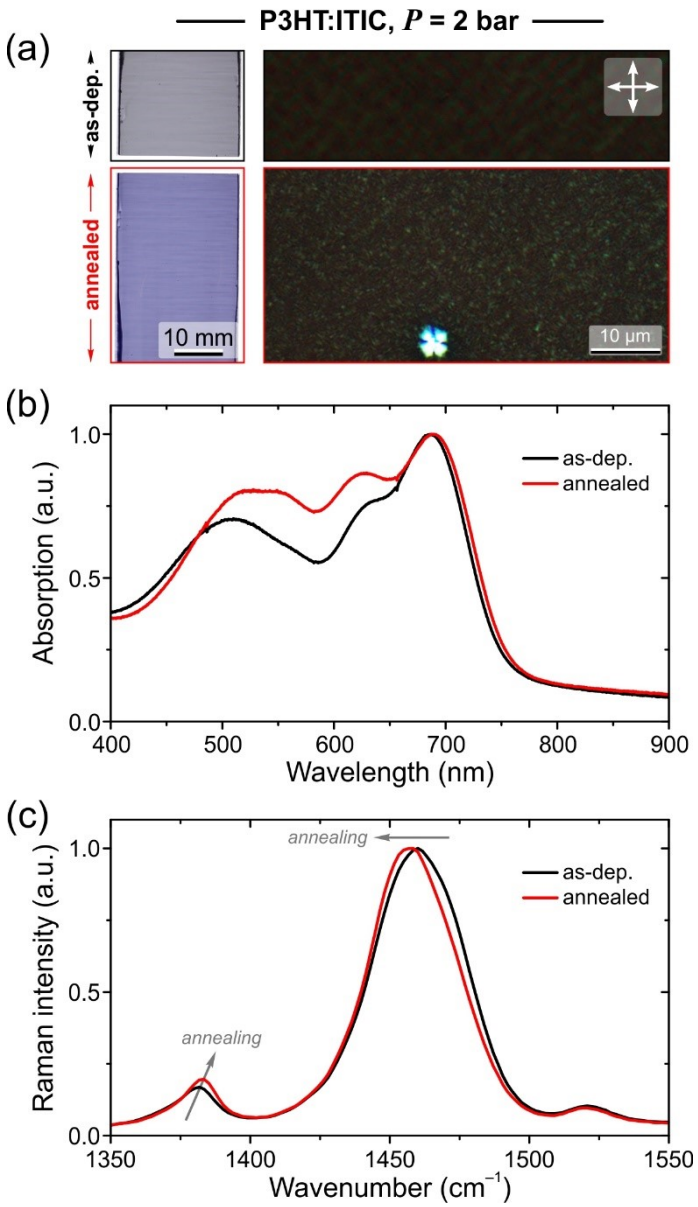

Figure S6. Recovery of crystallinity in vitrified P3HT:ITIC films by post-deposition annealing. Data is shown for P3HT:ITIC films coated using P = 2 bar: as-deposited ('as-dep.') and following post-deposition thermal annealing at 140 °C. (**a**) Transmitted-light images and the corresponding cross-polarised micrographs, (**b**) peak-normalised absorption spectra and (**c**) expanded view of the Raman spectra centred on the C=C in-plane symmetric stretching mode of P3HT.

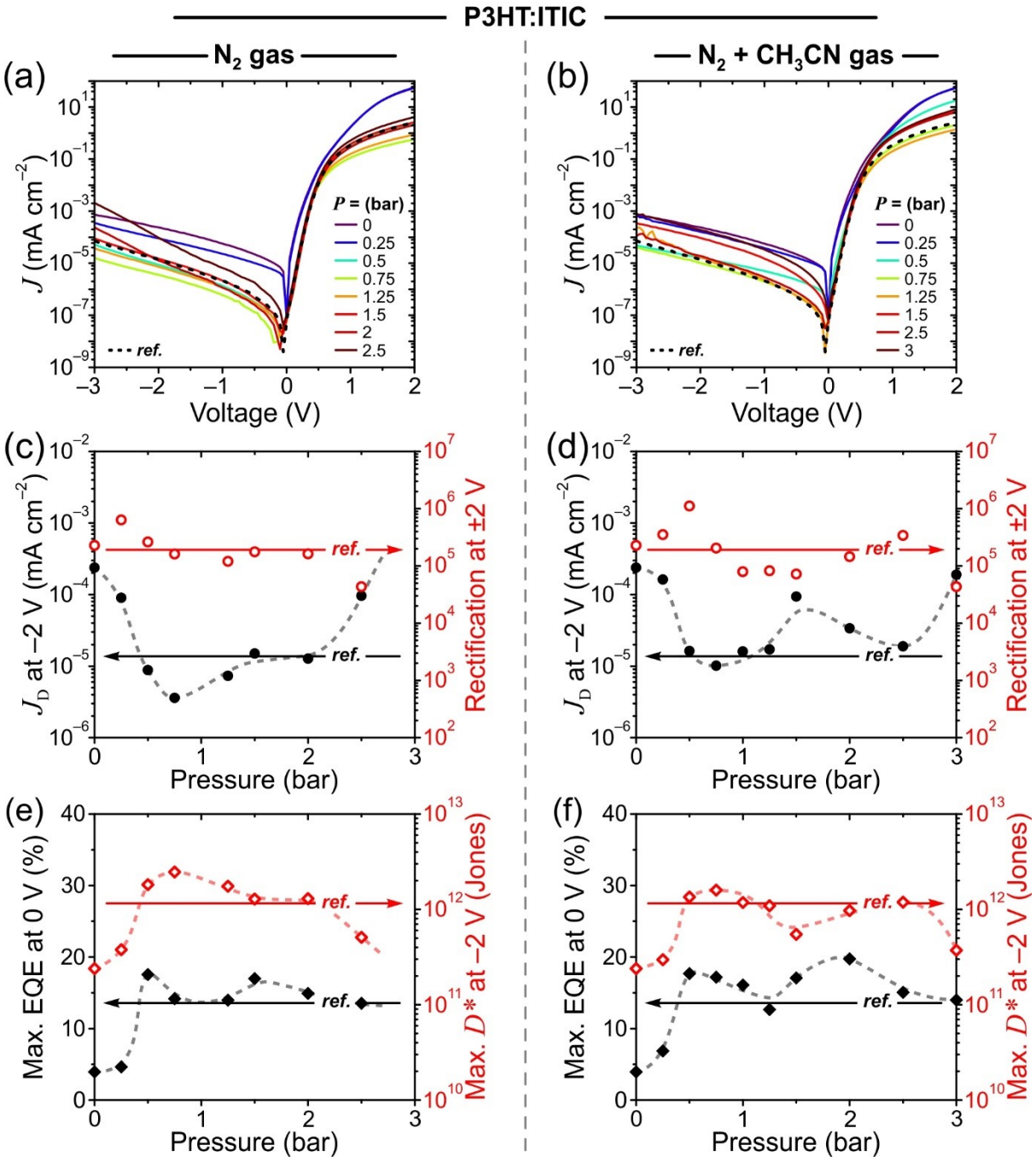

Figure S7. Characterization of OPDs based on blade-coated P3HT:ITIC active layers as a function of gas pressure. Data is shown for the two types of gases used: N_2 (*left column*) and acetonitrile-saturated N_2 (N_2 + CH_3CN; *right column*). (**a**,**b**) J-V curves recorded in the dark. The corresponding data for a reference ('ref.') device based on a spin-coated active layer is shown by the dotted line. (**c**,**d**) Dark-current J_D at –2 V and rectification at ±2 V; (**e**,**f**) maximum values of EQE at 0 V and specific detectivity D^* at –2 V . In both panels the corresponding values obtained for a reference spin-coated device are indicated by horizontal arrow markers. Dotted lines in (c–f) are a guide to the eye.

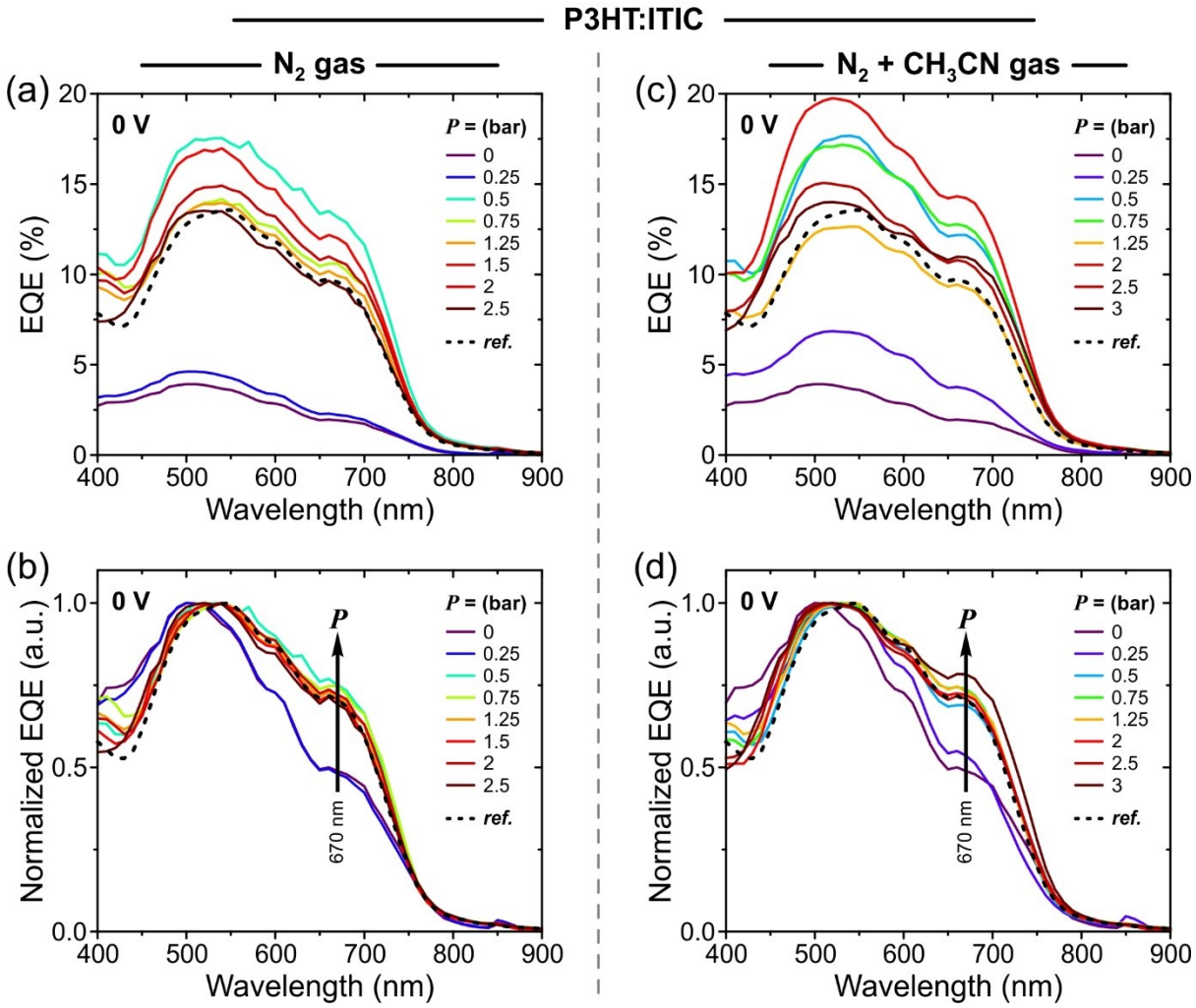

Figure S8. Zero-bias EQE spectra for blade-coated P3HT:ITIC OPDs as a function of gas pressure. Data is shown for two types of gases used: N_2 (*left column*) and acetonitrile-saturated N_2 (N_2 + CH_3CN; *right column*). (**a**,**c**) EQE spectra on absolute scale and (**b**,**d**) peak-normalized EQE spectra. The arrows highlight the relative increase of EQE for the acceptor band.

Table S1. EQE values for P3HT:ITIC OPDs for different active layer processing, highlighting the effect of drying gas selection (N_2 *vs.* N_2 + CH_3CN). Zero-bias EQE values are given for blade-coated (no gas and 0.5–2 bar gas pressure) and reference spin-coated devices.

Wavelength (nm)	**Maximum EQE (%)**			
	—	**N_2**	**N_2 + CH_3CN**	**spin-coated ref.**
	0 bar	*0.5–2 bar*	*0.5–2 bar*	—
520–540	3.9	15.5 ± 1.5	16.7 ± 2.1	13.6

670	1.9	11.3 ± 1.2	12.0 ± 1.5	9.6

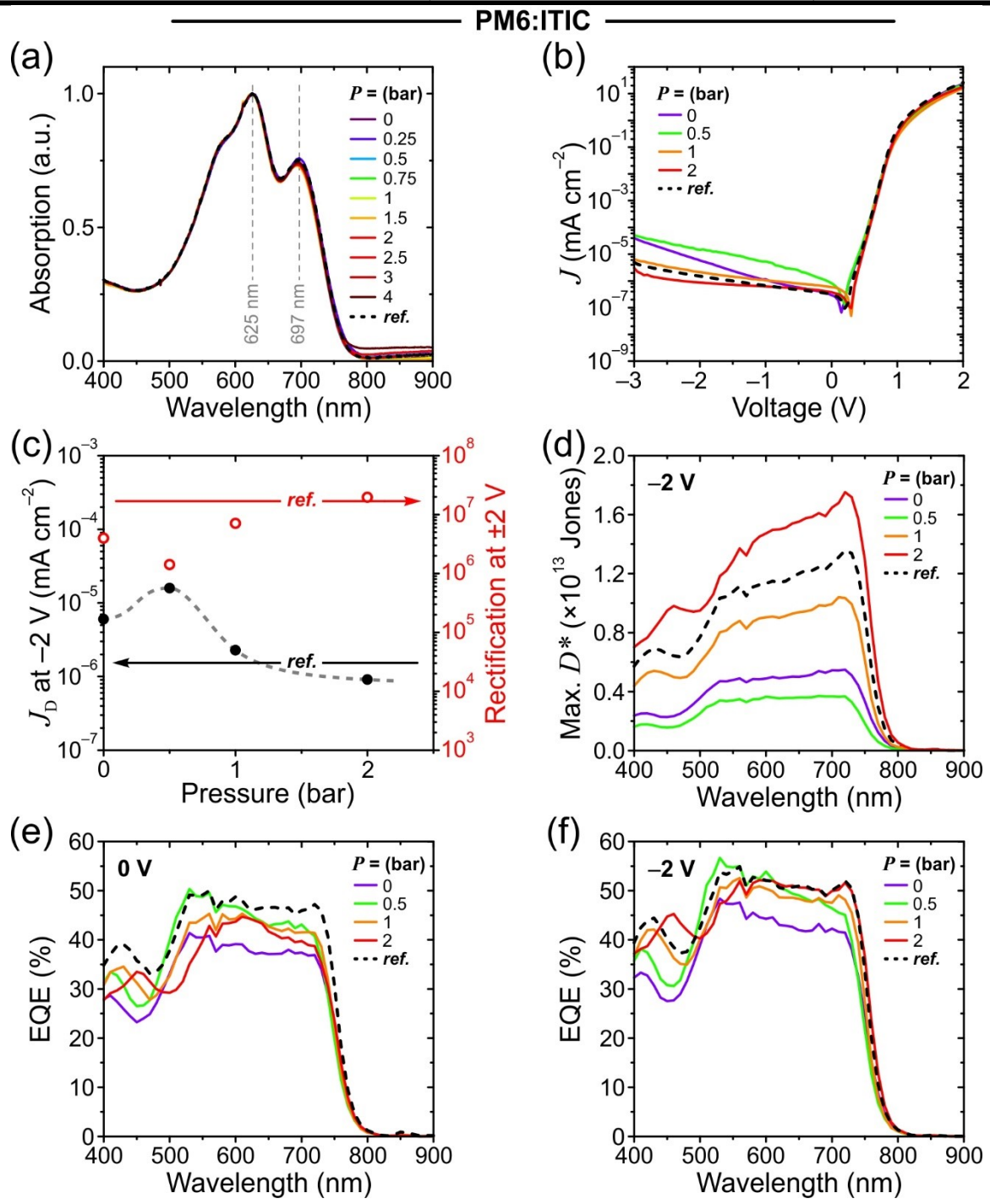

Figure S9. Characterization of blade-coated PM6:ITIC OPDs as a function of gas pressure. All active layers were post-crystallized by annealing at 100 °C for 10 min under N_2 atmosphere. Active layer thickness ≈ 150–180 nm for all devices. (**a**) Peak-normalized absorption spectra. Vertical markers indicate the absorption maxima of PM6 (625 nm) and ITIC (697 nm). (**b**) J-V curves recorded in the dark, and (**c**) the corresponding dark-current density J_D at –2 V and rectification at ±2 V. The corresponding J_D and R values obtained for a reference spin-coated device are indicated by horizontal arrow markers. Dotted gray line in (c) is a guide to the eye. (**d**) Estimated maximum specific detectivity D^* at –2 V. Also shown are the EQE spectra recorded under (**e**) zero bias and (**f**) –

2 V bias. In all cases, the data measured for a reference ('ref.') spin-coated device are shown by dotted black lines.

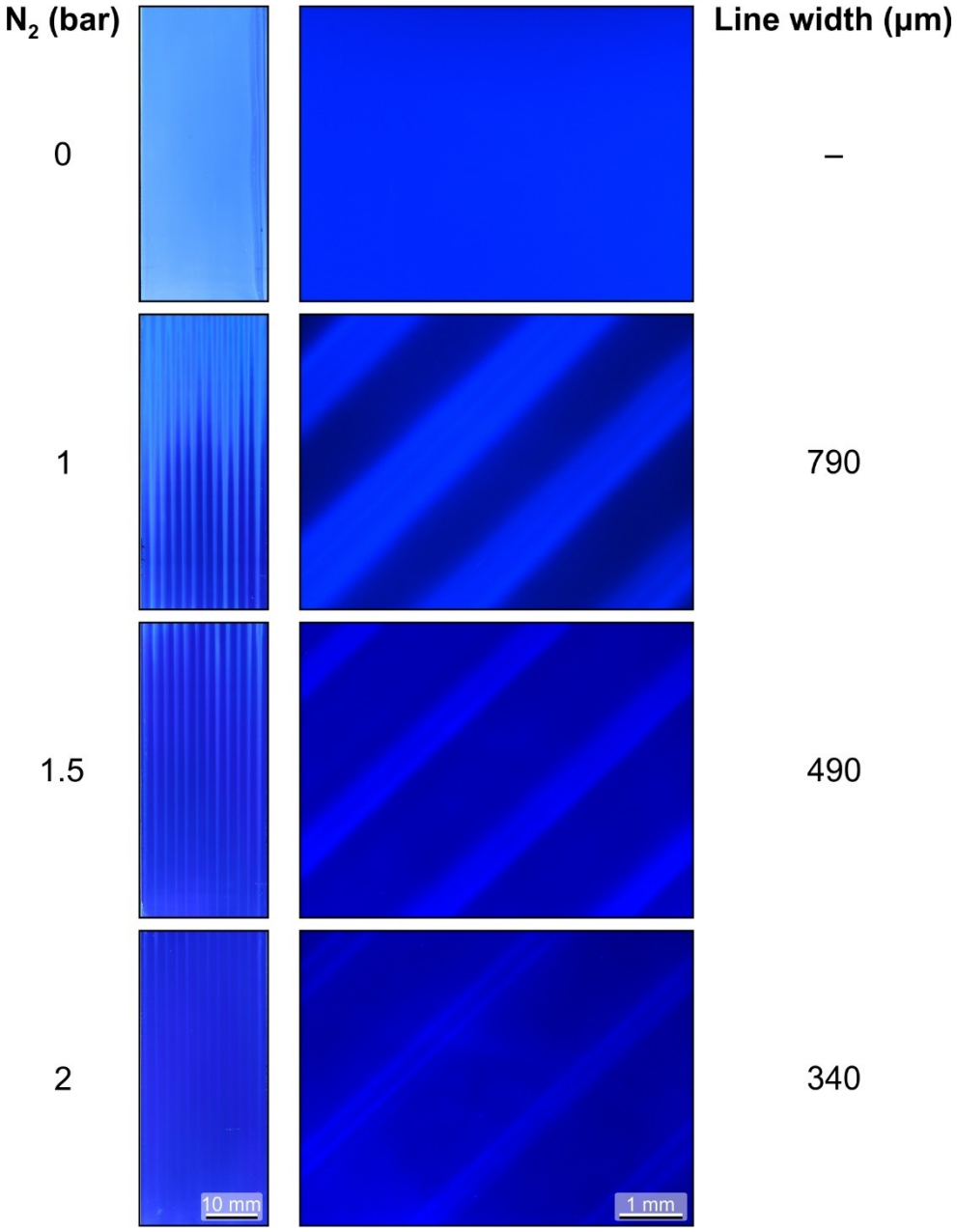

Figure S10. PFO films featuring one-dimensional (1D) chain-conformation-mediated photoluminescence patterns. *Left column*: large-area images of samples fabricated with N_2 flux directed via an array of nozzles at indicated pressures, recorded under UV-light (365 nm) illumination. *Right-column*: the corresponding small-area fluorescence micrographs recorded under UV-light illumination, highlighting the evolution of the width of β-phase lines (light-blue emission) with increasing pressure.

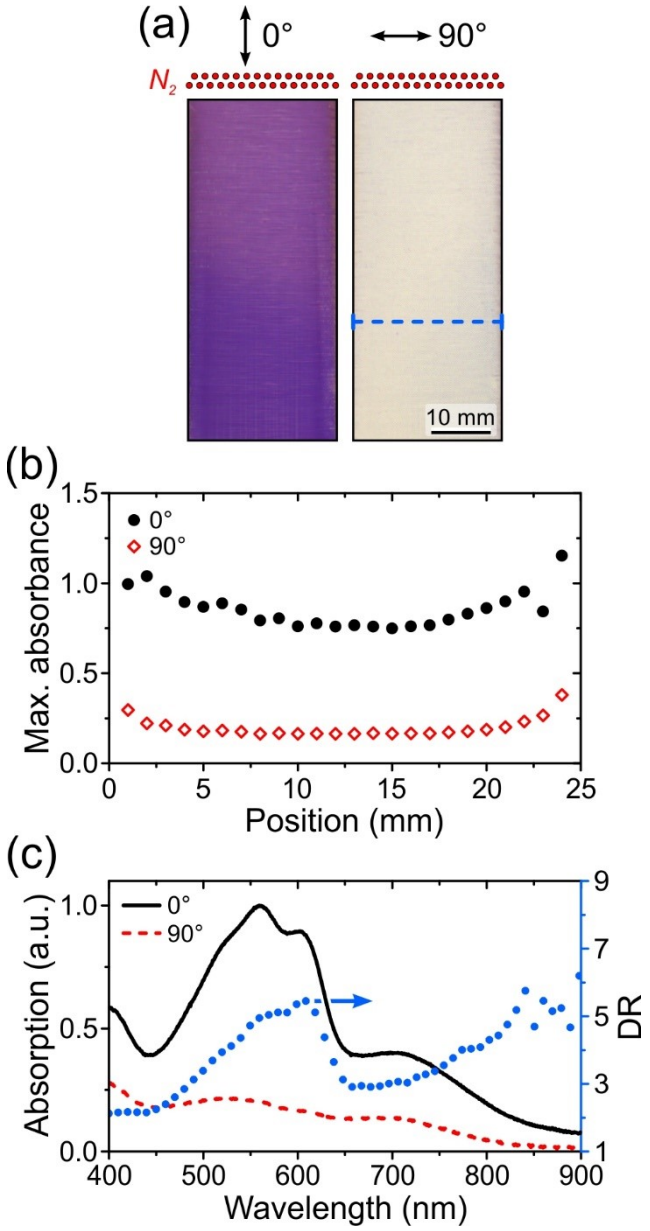

Figure S11. Reference, uniformly oriented P3HT:N2200 films. (**a**) Polarised transmitted-light images. Polarization of light with respect to the coating direction (top to bottom in the images) is indicated by ↔. (**b**) Profiles of maximum P3HT absorption across the width of the film, as indicated by the dashed line in (a), recorded with light polarized at 0° and 90° with respect to the coating direction. (**c**) Polarised absorption spectra recorded at the centre of the film (left ordinate) and the corresponding dichroic ratio spectra (DR; right ordinate). Film was deposited from 1.3% solution in chloroform:TCB (1:0.22 wt/wt) using coating speed = 5 mm s^{-1} and N_2 flow (P = 2 bar) directed via an array of nozzles (depicted by red circles in (a)).

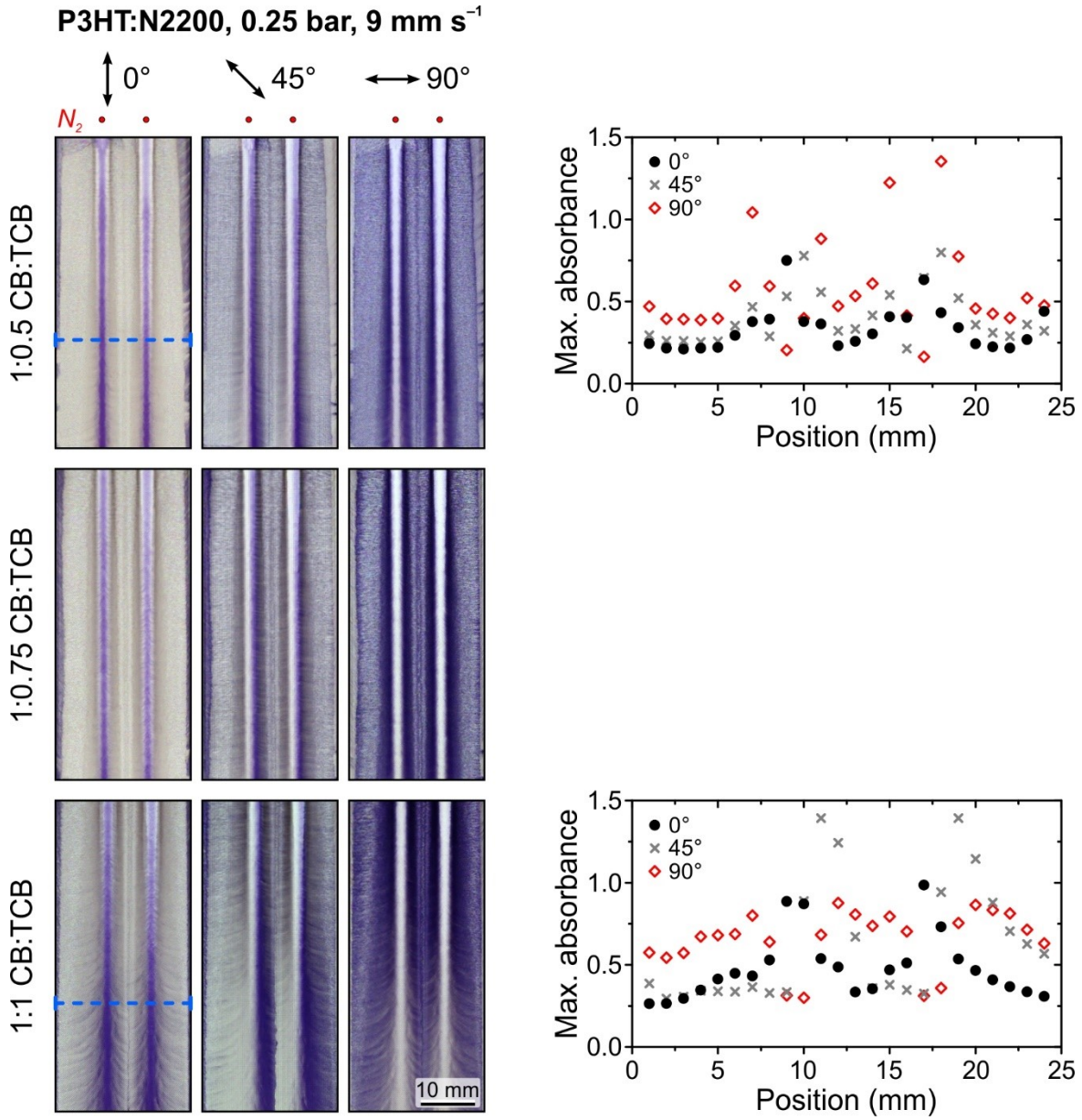

Figure S12. 2D-oriented P3HT:N2200 films: effect of CB:TCB ratio. Images of blade-coated films recorded under polarized transmitted-light illumination (polarization direction indicated by ↔). Films were blade-coated from 1.3% solutions in CB:TCB (wt/wt ratios spanning 1:0.5 to 1:1; as indicated) at 30 °C and coating speed = 9 mm s^{-1}. Coating direction is top to bottom in the images. N_2 gas at 0.25 bar pressure was directed via two nozzles (0.75 mm diameter; 8 mm apart), as indicated by the red circles. Local preferential chain orientation direction is revealed by polarization-dependent changes in optical density. Also shown are the corresponding profiles of maximum P3HT absorbance across the width of the film (as indicated by the dashed lines in the respective images) recorded at different polarization angles.

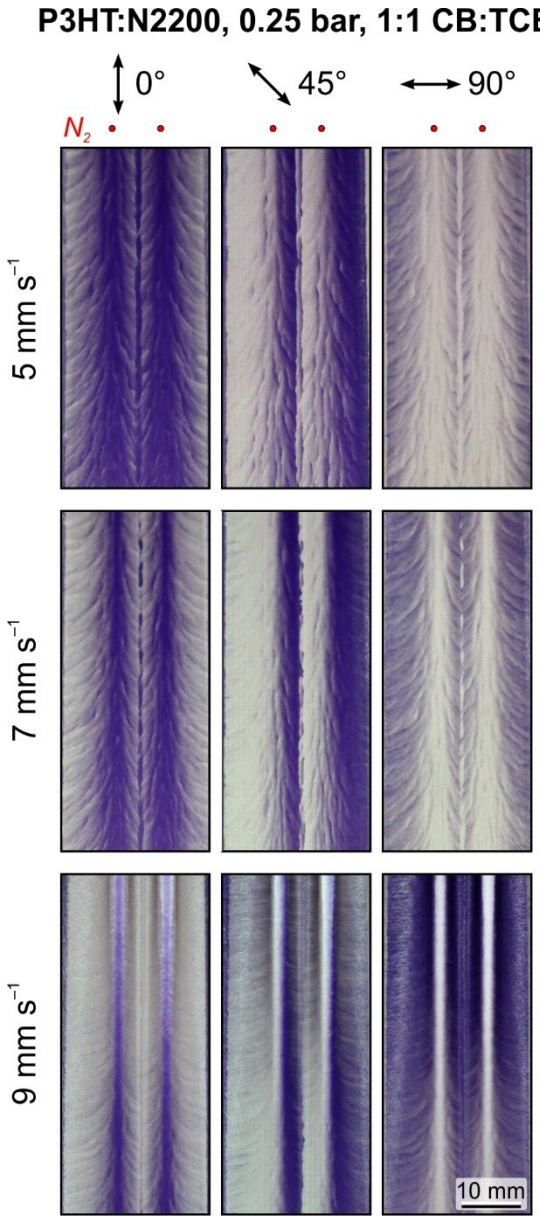

Figure S13. 2D-oriented P3HT:N2200 films: effect of coating speed. Images of blade-coated films recorded under polarized transmitted-light illumination (polarization direction indicated by ↔). Films were blade-coated from 1.3% solutions in 1:1 CB:TCB at 30 °C and coating speed ranging from 5 to 9 mm s^{-1} (as indicated). Coating direction is top to bottom in the images. N_2 gas at 0.25 bar pressure was directed via two nozzles (0.75 mm diameter; 8 mm apart), as indicated by the red circles. Local preferential chain orientation direction is revealed by polarization-dependent changes in optical density.